# Land Use and Land Cover (LULC) Assessment within the Batanes Protected Landscapes and Seascapes

**Nova D. Doyog[1]\*, Roscinto Ian C. Lumbres[1], Lynn J. Talkasen[2],
and Deign Frolley C. Soriano[3]**

[1]College of Forestry/Center for Geoinformatics, Benguet State University,
La Trinidad, Benguet 2601 Philippines
[2]College of Agriculture/Center for Geoinformatics, Benguet State University,
La Trinidad, Benguet 2601 Philippines
[3]Department of Biology, College of Science, University of the Philippines Baguio,
Governor Pack Road, Baguio City 2600 Philippines

**Declared protected areas have ecologically important landscapes that must be conserved and protected. Status of protected areas could be monitored through land use and land cover (LULC) assessments. LULC offers baseline data for integrated land use planning and improvement of existing policies are therefore necessary to be conducted. This study was conducted to monitor the existing LULC of six islands within the Batanes Protected Landscapes and Seascapes (BPLS) through a machine learning (ML)-based random forest (RF) classifier using multi-sourced data such as Landsat imageries' surface reflectance (SR), Landsat-derived land surface temperature (LST), and global ecosystem dynamic investigation (GEDI)-derived height (Ht) metrics and to determine the effects of the LST and Ht metrics to LULC classification. Four layer stacked images with different features were analyzed – including SR, SR-LST, SR-Ht, and SR-LST-Ht. The result of the LULC classification showed an accuracy based on Macro F1-score and Kappa (K) of 0.81 and 0.83, 0.83 and 0.86, 0.86 and 0.89, and 0.93 and 0.94, for SR, SR-LST, SR-Ht, and SR-LST-Ht, respectively. When compared to the existing global-scale LULC, this study has higher accuracy than the GLAD and ESRI products, which have Macro F1-scores and K-values of 0.73 and 0.71, and 0.59 and 0.64, respectively. To conclude, the inclusion of LST and Ht information in addition to SR data in LULC classification can improve the accuracy by up to 12% and 11% based on Macro F1-score and K, respectively. The result of this study can serve as a reference for achieving improved and reliable LULC information that is necessary for monitoring fluctuations of the global earth's resources and comprehensive LULC planning. In addition, the technique used in this study can serve as a reference in generating reliable LULC information that can aid in the sustainable implementation of policies, rules, and regulations intended for declared protected areas like BPLS.**

Keywords: GEDI-height product, global-scale LULC, optical data, protected areas, thermal sensing

## INTRODUCTION

Land use and land cover (LULC) monitoring is crucial in forest ecosystem conservation and protection because it can identify potential areas that are at risk of land use conversion and deforestation (Tarazona and Miyasiro-López 2020), therefore enabling effective forest management and conservation planning. LULC monitoring provides information needed for biodiversity assessment (Disperati and Virdis 2015), fire management (Vilar *et al.* 2021), and environmental impact assessments. Further, LULC information is also one of the key references for policymaking, planning,

and implementation of management strategies that are appropriate for combating the growing impacts of climate change and other environmental concerns (FAO 2016). With the crucial role of LULC monitoring, understanding LULC dynamics is essential, and it needs to be of as high accuracy as possible. Updated, precise, and accurate LULC monitoring is needed and can be achieved through multi-temporal LULC mapping. By analyzing changes in LULC over time, multi-temporal LULC mapping enables accurate detection of land cover changes – including deforestation, urban expansion, agricultural expansion, and natural disturbances (Wiederkehr *et al.* 2020; Clarin *et al.* 2021; Doyog *et al.* 2021; Baig *et al.* 2022). These data contribute to a better understanding of the dynamics of the Earth's surface and support decision-making for sustainable land management, conservation, and resource planning. In addition, multi-temporal LULC mapping enables capturing seasonal variability because different land cover types exhibit seasonal variability due to factors such as vegetation growth, phenology, and natural cycles. And lastly, long-term trends of LULC changes are also identified when multi-temporal LULC mapping is conducted. By analyzing historical LULC data, it becomes possible to understand the patterns, rates, and drivers of land cover change over an extended period. This information helps in predicting future trends (Baig *et al.* 2022) and assessing the effectiveness of conservation and management interventions.

To conserve biodiversity, protect and maintain the ecological integrity of landscapes and seascapes, and prevent the continuous conversion of LULC, the Philippines established a declaration of protected areas. As per the enactment of the expanded National Integrated Protected Areas System or e-NIPAS Act in 2018, the Protected Area Management Board oversees 94 protected areas in the Philippines. In addition, other protected areas were declared through other legislations like the Batanes Protected Landscapes and Seascapes (BPLS). Part of monitoring the effectiveness of the declaration of the protected areas can be provided by conducting LULC monitoring.

LULC mapping can be performed using various techniques – from traditional to advance. Before the evolvement of advanced techniques, LULC mapping was first conducted traditionally through visual interpretation of images; however, it is subjective, time-consuming, and suitable for small-scale mapping. On the other hand, advanced techniques involve the use of machine learning (ML) and remote sensing (RS) data (Li *et al.* 2012; Basheer *et al.* 2022). ML algorithms such as artificial neural networks (ANNs), convolutional neural networks, decision trees, random forest (RF), support vector machine (SVM), k nearest neighbor (kNN), and maximum likelihood classifiers (MLC) are increasingly

being used for LULC mapping. These algorithms learn from training data to automatically classify land cover based on spectral, textural, and contextual features and can handle large datasets enabling accurate and efficient land cover classification and can improve accuracy when trained with appropriate training samples.

For RS-based LULC mapping, several types can be utilized, depending on the available resources, resolution, and the desired level of accuracy. Satellite imagery is a primary source of data for LULC mapping – which are either high-resolution (1-5m) like WorldView, GeoEye, or Pleiades (Zhang and Kerekes 2011; Sertel *et al.* 2022), medium-resolution satellite data (10–30 m) like Landsat or Sentinel-2 (Estoque and Maruyama 2011; Merida and Perez 2017; Doyog *et al.* 2021), or low-resolution satellite data (> 30 m) like NASA (National Aeronautics and Space Administration) Terra or Aqua MODIS (Song *et al.* 2011; Gebrejewergs *et al.* 2018). Other RS data include aerial photographs and those that are acquired by active remote sensors like light detection and ranging (LiDAR) and synthetic aperture radar.

Despite the advantages and high performance that advanced techniques offer, LULC classification can lead to many setbacks. The presence of clouds in satellite imagery, which alters the correct surface reflectance (SR) of the earth's surface is unavoidable, so using SR information alone is not enough to achieve highly accurate results. The high degree of similarity in spectral information can also lead to poor classifications of individual classes. However, the use of other metrics such as vegetation indices, biological information like canopy height and leaf area index, and topographic features like elevation, slope, and aspect can help solve this problem. The use of vegetation indices like the normalized difference vegetation index (NDVI) in combination with the Savitzky-Golay filter (Mi *et al.* 2019), enhanced vegetation index, normalized difference water index (NDWI), soil-adjusted vegetation index, and NDVI (da Silva *et al.* 2020) in the field of LULC classification has been practiced and provided satisfactory results. From being merely used as an input feature, it has also been noted to increase the accuracy of LULC classification, as shown in the works of Sinha *et al.* (2015), wherein they used the thermal integrated vegetation and advanced thermal integrated vegetation indices as an added feature in combination with the spectral features of the Landsat 7 image. The Ht information also helped in the LULC classification that was conducted by Gxumisa and Breytenbach (2017) and the works of Xie *et al.* (2019) showed that even slope information had a great contribution to the improvement of the quality of the LULC classification.

In addition, several methods can be used to address the issue of cloud cover in satellite imagery such as cloud masking and replacement. Clouds can significantly impact

LULC classification, so they should be removed from the input data as much as possible before LULC classification is performed.

This study was conducted to assess the LULC of the six islands within the BPLS using SR of Landsat images, LST, and Ht information as input data and ML-based RF as the classifier. In addition, this study is aimed to determine and compare the effects of integrating Ht, LST, and SR on LULC classification. Hence, a total of four stacked images are being compared in this study – namely, SR, SR-Ht, SR-LST, and SR-Ht-LST. Six classes are being classified – namely, agriculture (Ag); bare land (Bl), which includes those non-vegetated areas, sand, and rocks; built-up (Bu), which consists of buildings and road networks; forest (F); grassland (Gl); and water (W), which includes the inland water and ocean.

## MATERIALS AND METHODS

### Study Site
The Batanes group of islands and islets is located in the northernmost part of the Philippines. The northernmost island called Y'ami is 141 km away from the southern tip of the main island of Taiwan and 98 km away from the nearest Taiwan island named Lesser Orchid Island. Basco, which is the capital town, is approximately 280 km away from Aparri, Cagayan, 860 km away from Manila and 190 km away from the southernmost part of the main island of Taiwan.

Along with its surrounding waters, the islands and islets were included as one of the 10 Integrated Protected Area System sites of the Philippines in 1994 and were declared a protected landscape and seascape through Presidential Proclamation No. 335, s. 1994 and Republic Act No. 8991, also known as the Batanes Protected Area Act of 2000 – which aimed to protect, preserve, and conserve the islands' diverse terrestrial and marine ecosystem. The BPLS consists of 10 islands – namely, Y'ami, North Island, Mavudis, Siayan, Itbayat, Dinem, Batan, Sabtang, Vohas, and Dequey. Only the three main islands are inhabited (Batan, Itbayat, and Sabtang). According to the 2020 population data (PSA 2020), Batan has the highest population, accounting for 74.38% of the total population. Itbayat comes next with 16.61%, and Sabtang has the smallest population making up 9.01%. In terms of population density, Batan has the highest density at 176/ km$^2$, followed by Sabtang at 38/km$^2$, and Itbayat at 42/ km$^2$, respectively. The climate of the region is classified as tropical rainforest according to the Köppen climate classification. It is characterized by unpredictable rainfall distributed throughout the year. The average yearly temperature is 26.61 ºC. The coldest month is January, with temperatures ranging from 20–26 ºC and an average of 22.52 ºC. On the other hand, the hottest month is June, with temperatures ranging from 26–32 ºC and an average of 29.39 ºC. Due to its geographical location, the area is highly susceptible to disturbances such as typhoons, strong winds, and sea-level rise (Yumul *et al.* 2011). This study primarily focuses on the three inhabited islands – as well as Dinem, Vohas, and Dequey islands (Figure 1).
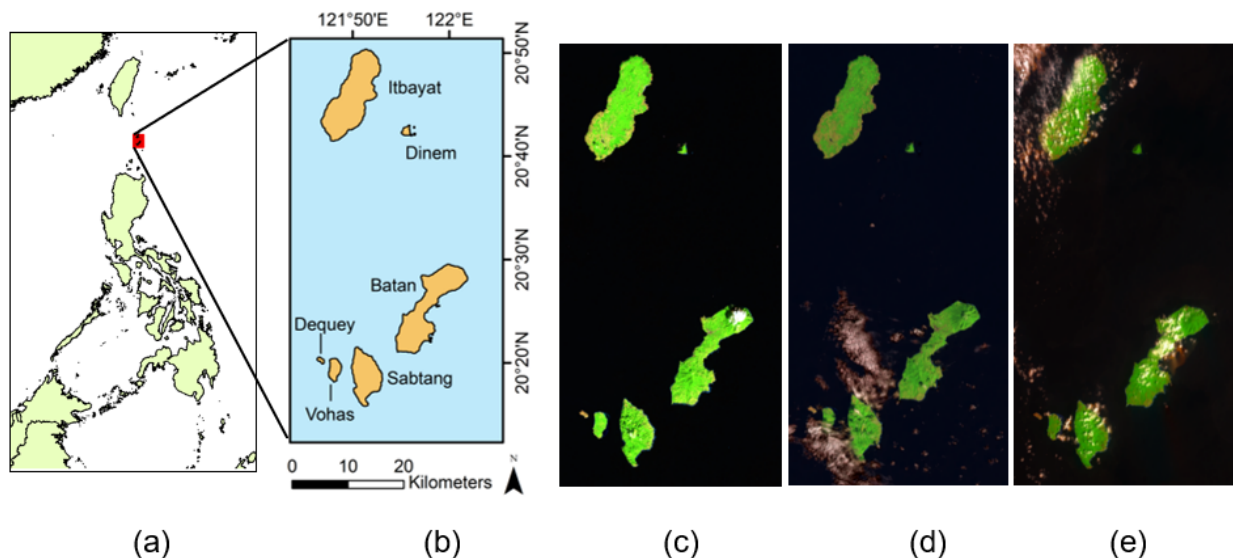


**Figure 1.** Location of the BPLS in the Philippines (a), the six islands of BPLS that were subjected to LULC classification (b), and the multi-temporal Landsat images of the islands showing various distributions of cloud cover (c–e). The images (c–e) were displayed using bands 6, 5, and 4 for RGB, respectively.

**Data Acquisition**

**SR data.** Table 1 summarizes the features that were used in this study with their corresponding source data. The Bands 1–7, modified normalized difference water index (MNDWI), and LST were derived from Landsat 8 and 9 images, and the Ht information was derived from the GEDI-based global canopy height (Potapov *et al.* 2021).

With the reason that no single satellite image with a cloud-free cover is available in the archived data, four multi-temporal Landsat images (Landsat 8 and 9) were used in this study. Level 2 products of Landsat 8 images acquired in February 2019, January 2020, and March 2021 and Landsat 9 images acquired in 2022 (March) were downloaded freely at the USGS website (https//:www.usgs.earthexplorer.com). Both Landsat 8 and 9 carry 2 instruments – namely, the operational land imager (OLI) and the thermal infrared sensor (TIRS). OLI has eight multi-spectral bands – namely, Bands 1–7 and 9 with 30-m spatial resolution – and one panchromatic band (Band 8) with 15-m spatial resolution. The TIRS has two thermal bands – namely, 10 and 11 with 100-m spatial resolution. Landsat 8 was launched on 11 Feb 2013, and Landsat 9 was launched on 27 Sep 2021.

Before image classification, the pansharpening and cloud masking techniques were performed on the images. The NNDiffuse model was used for the pansharpening. The purpose of pansharpening is to create a high-resolution colored image by merging a single band high-resolution black and white image (panchromatic) and a medium or low-resolution multi-spectral image. After the pansharpening process, manual cloud masking was performed to remove cloud cover and cloud shadow in each of the four Landsat images. Table 2, Column 1 shows the final satellite images that were used for LULC mapping of each island after the cloud masking; Columns 2–5 pertain to the other details of the satellite images.

In this study, the MNDWI was incorporated as an additional feature. The MNDWI was calculated using the green and SWIR bands (the formula is provided in Table 1), following pansharpening and cloud masking, to assist in the identification of water areas. Merida and Perez (2017) have previously highlighted the challenge of classifying shorelines accurately, as they are often misclassified as built-up areas. While additional spectral indices could potentially enhance reliable LULC mapping, they were not utilized in this study, as spectral indices are typically derived from the optical data's spectral bands. Instead, the focus of this study was on examining the impact of LST and Ht information on LULC classification. The Bands 1–7, along with the MNDWI, were stacked together and collectively referred to as SR features.

**Landsat-based LST data.** The TIRS of Landsat 8 and 9 have two thermal bands (Bands 10 and 11) that are purposely for measuring the emitted radiation based on emissivity and are further used for the calculation of LST. For this study, the single-channel method using Band 10 was used for the retrieval of LST because it has higher accuracy than Band 11, and Band 11 has some uncertainties, as reported by the Landsat 8 team in their Landsat 8 Data Users Handbook version 5 (Zanter 2019). A series of steps were performed to retrieve the LST in each image. The top of atmospheric spectral radiance was calculated first using Equation 1, followed by the conversion of TOA to brightness temperature using Equation 2, calculation of the proportion of vegetation (Pv) using Equation 3, and emissivity (ε) using Equation 4, and lastly, the computation of the LST using Equation 5. In Equation 1, TOA is the top of the atmosphere, ML is the band-specific multiplicative rescaling factor from the metadata, Qcal is the quantized calibrated pixel value in DN, and AL is the band-specific additive rescaling factor from the metadata. In Equation 2, BT is the brightness temperature, K1 is the band-specific thermal conversion

**Table 1.** List of data for the LULC classification within the BPLS.

| Feature | Source data | Remarks |
|---|---|---|
| SR (Bands 1–7 and MNDWI) | Landsat 8 and 9 images<br><br>(2019, 2020, 2021, 2022) | ➢ Multi-temporal; 15-m spatial resolution after the pansharpening using panchromatic data (band 8).<br>➢ MNDWI = (Green – SWIR) / (Green + SWIR)<br>MNDWI = (B3 – B6)/ (B3 + B6) |
| LST | Landsat 8 and 9 images<br><br>(2019, 2020, 2021, 2022) | ➢ Multi-temporal; 15-m spatial resolution<br>➢ 2 thermal bands (10 and 11) but only band 10 was used because band 11 has some uncertainties (Zanter 2019).<br>➢ NDVI = (NIR – Red) / (Red + NIR)<br>NDVI = (B5 – B4)/(B4 + B5) |
| GEDI-derived Ht information (2019) | Potapov *et al*. (2021) | ➢ 30-m spatial resolution but was resampled to 15 m to be consistent with the SR and LST<br>➢ LULC classes have different height information |

**Table 2.** Relevant information on the satellite image of the study sites within the BPLS.

| Island/s | | Product ID | Acquisition date/ scene center time | LCC | Sun azimuth/ elevation |
|---|---|---|---|---|---|
| Itbayat and Dinem |  | LC09_L2SP_116046_20220309_20220311_02_T1 | 2022-03-09/02:15:51.8678399Z | 8.32 | 130.70048064/54.03925963 |
| Itbayat and Dinem |  | LC08_L2SP_116046_20200123_20200823_02_T1 | 2020-01-23/02:15:58.3900269Z | 27.97 | 145.03061488/42.34348824 |
| Batan |  | LC09_L2SP_116046_20220309_20220311_02_T1 | 2022-03-09/02:15:51.8678399Z | 8.32 | 130.70048064/54.03925963 |
| Batan |  | LC08_L2SP_116046_20210330_20210409_02_T1 | 2021-03-30/02:15:37.0830079Z | 33.54 | 120.63542419/60.58038512 |
| Sabtang, Vohas, & Dequey |  | LC08_L2SP_116046_20190221_20200829_02_T1 | 2019-02-21 /02:15:33.2529140Z | 20.16 | 136.52609561/48.99528843 |

Note: LCC is land cloud cover

constant (in W/m² * ster * µm), K2 is the band-specific thermal conversion constant (in Kelvin), L is the spectral radiance, and 273.15 is the conversion factor from Kelvin to degree Celsius. In Equation 3, Pv is the proportion of vegetation and NDVI is the normalized differential vegetation index. In Equation 4, ε is the land surface emissivity, whereas 0.004 and 0.986 are the constant and correction value. Lastly, in Equation 5, w is the wavelength of emitted radiance (thermal band), with *p* = 14380.

$$TOA(L) = M_L * Q_{cal} + A_L \qquad (1)$$

$$BT = \left[ \frac{K_2}{\left( ln\left(\frac{K_1}{L}\right) + 1 \right)} \right] - 273.15 \qquad (2)$$

$$P_v = \left[ \frac{(NDVI - NDVI_{min})}{(NDVI_{max} - NDVI_{min})} \right]^2 \qquad (3)$$

$$\varepsilon = 0.004 * P_v + 0.986 \qquad (4)$$

$$LST = \left| \frac{BT}{\left[ 1 + W * \left( \frac{BT}{p} \right) \right]} \right| * Ln(\varepsilon) \qquad (5)$$

**GEDI-based Ht data.** The Ht information used in this study was retrieved from the 2019 global canopy height product that was generated using the integration of GEDI and Landsat data (Potapov *et al.* 2021). The GEDI data was collected in April–October 2019, and the Landsat analysis-ready data were processed using Landsat Collection 1 data from 1997–2019. The GEDI, which is a joint mission of NASA and the University

of Maryland, is the first space-borne LiDAR that was launched in 2018 purposely for canopy height retrieval; however, it has a ground footprint of 25 m in diameter, and every footprint has a distance of 60 m across track and 600 m along track. Therefore, using the GEDI-derived Ht information, canopy height estimations with the aid of regression models and ancillary data should be performed to generate wall-to-wall canopy height information. The 2019 global canopy product has a spatial resolution of 30 m and is freely available for use and can be downloaded at https://glad.umd.edu/dataset/gedi. For this study, to be consistent with the spatial resolution of the SR, the Ht product was resampled from 30 to 15 m using the nearest technique. The canopy height product, however, did not cover the entire Batanes Landscape, especially the part of Mt. Iraya on Batan Island (Figure 2). Only the 2019 Ht information was used in this study. Nevertheless, considering a business-as-usual scenario, the canopy height rarely changes significantly from 2019–2022; therefore, using Ht information derived only in 2019 is reasonable for this study. Further, at present, the wall-to-wall canopy height information of BPLS is not yet available for 2021 and 2022.

**Reference data.** The training and validation data used in this study were collected by visually inspecting high-resolution images from the Google Earth Pro desktop application. Random selection was employed to gather the data. Seed points were generated using a random distribution across the entire study site, and each seed point was extended by 1 pixel on all sides, resulting in a total of 9 pixels per seed point. This random selection approach ensured a higher frequency of LULC classes with greater representation across the area. The validation dataset consisted of the following proportions: 7.09% agriculture, 21.41% bareland, 4.29% built-up, 30.69% forest, 13.71% grassland, and 22.81% water.

## LULC Classification

The LULC classification was performed using the RF classifier, which is a non-parametric ML algorithm that is based on decision trees (Breiman 2001). The random sample selection or the bagging process of RF paves the way for achieving uncorrelated decision trees. The success of RF highly depends on using uncorrelated decision trees. One of the unique features of the RF classifier is ranking the variable importance using mean decrease accuracy (MDA) and the mean decrease Gini (MDG) as criteria. The MDA expresses how much accuracy the model losses by excluding each variable. The MDG is a measure of how each variable contributes to the homogeneity of the nodes and leaves in the resulting RF. The higher the MDA or the MDG score, the higher the importance of the variable in the model. Variables of low importance or those that do not contribute much to the outcome of the classification are supposedly not being used.

The applicability and good performance of the RF in LULC classification were already proven by previous studies (Gislason *et al.* 2006; Ghimire *et al.* 2010; Guo *et al.* 2011; Havens *et al.* 2013; Puissant *et al.* 2014; Nitze *et al.* 2015; Xia *et al.* 2015). Using the RF classifier, the LULC classification was performed on all five cloud-free images of the study site. The image mosaicking technique using the mean was performed after the image classification.

## Accuracy Assessment

The generated LULC maps using the different features were compared based on the performance that was evaluated using precision (Equation 6), recall (Equation 7), F1-score (Equation 8), Macro F1-score, kappa coefficient (K) (Equation 9), and overall accuracy as criteria. In Equations 6 and 7, true positives are the observations that were correctly predicted by the model,
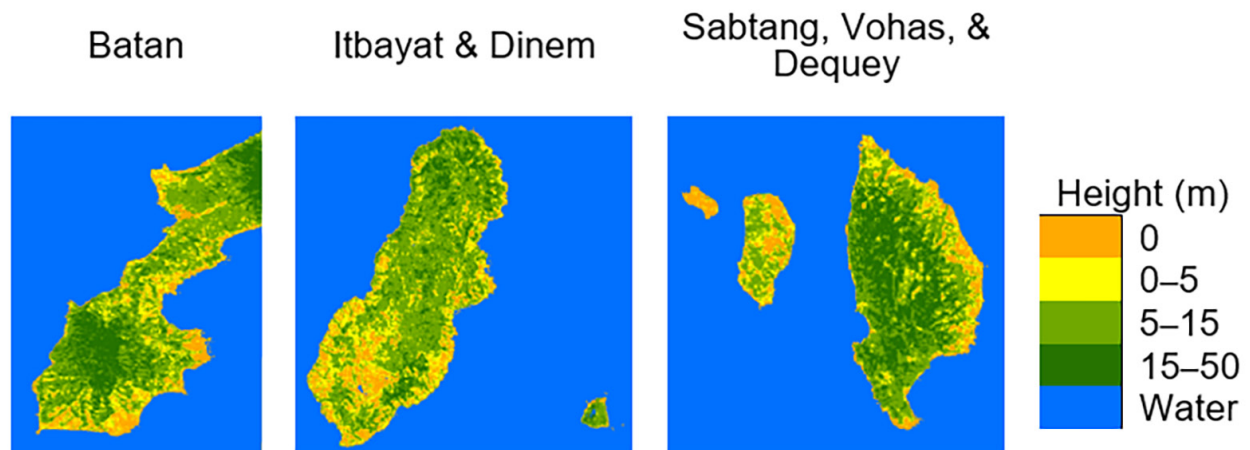


**Figure 2.** The GEDI-based height information of the study sites.

false positives are those predicted data that were included in a class but do not belong to the class, and false negatives are those that were omitted to a particular class and misclassified as a different class. Precision is a measuring criterion that assesses the quality of the model, whereas recall measures the number of relevant results that the model returns – either relevant or irrelevant. F1-score is calculated from the individual precision and recall of the classes and the Macro F1-score is the average of all the per-class F1-scores. The K measures the agreement between classification and truth values and ranges from 0 (worst) to 1 (best).

Lastly, the results of the LULC classification in this study were compared with the existing global-scale LULC products such as the 2019 Global Land Analysis and Discover (GLAD) product (Hansen *et al.* 2022) and the 2020 Environmental Systems Research Institute (ESRI) product (Karra *et al.* 2021). The ESRI product was generated using the artificial intelligence technique,

particularly the deep learning model, and has a spatial resolution of 10 m. The ESRI product was produced using the visible bands (blue, green, red), near-infrared, and the two shortwave infrared features of Sentinel-2 and has an overall global accuracy of 86%. On the other hand, the GLAD LULC product is a 30-m resolution map produced using Landsat satellite imagery and topographical data and various algorithms such as entropy-based classification trees and the sum of squares-based regression trees. The GLAD LULC product has an overall global accuracy of 78.35%. The ESRI product covers the whole BPLS, but the GLAD LULC does not specifically on the part of Mt. Iraya because it used the GEDI-height product as ancillary data. The accuracy and extent of the area covered by the individual classes were compared. The area coverage of the LULC maps in this study and the ESRI product was adjusted to be consistent with the GLAD product. The overall flowchart of the processes is summarized in Figure 3.
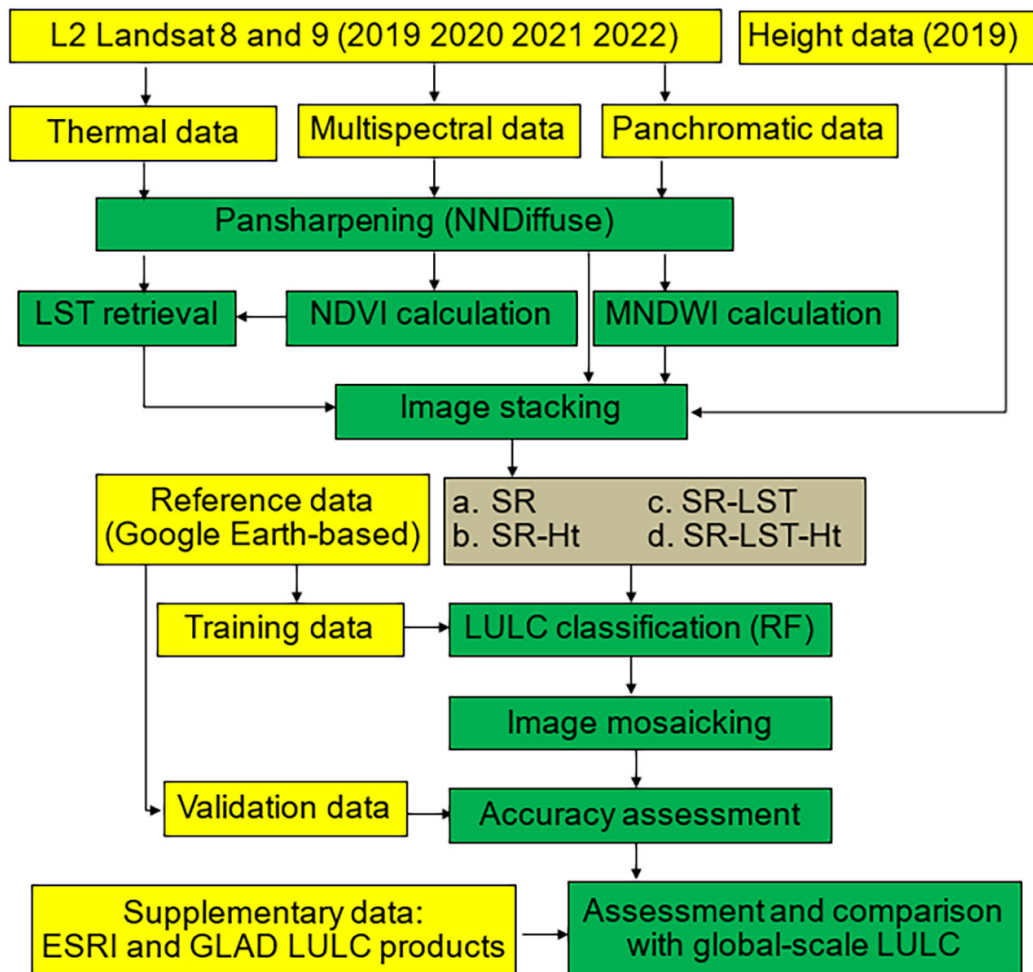


**Figure 3.** The process used in the comparison of the effects of the features on the LULC classification.

$$Precision = \frac{True\ positives}{(True\ positives + False\ positives)} \quad (6)$$

$$Recall = \frac{True\ positives}{(True\ positives + False\ negatives)} \quad (7)$$

$$F1 - score = 2x \left[ \frac{(Recall\ x\ Precision)}{(Recall + Precision)} \right] \quad (8)$$

$$\hat{K} = \left[ \frac{(Observed\ agreement - Expected\ agreement)}{(Total\ observations - Expected\ agreement)} \right] \quad (9)$$

## RESULTS

Figure 4 shows the LULC classification map of the study sites using different input data. From the LULC maps, the study sites are majority covered with water – followed by forest, grassland, bareland, agriculture, and built-up, respectively. On average, the study sites covered 66.24% of water, 21.05% of forest, 7.93% of grassland, 2.31% of bareland, 1.79% of agriculture, and 0.67% built-up. The low area coverage of built-up indicates that the islands of Batanes are not yet heavily urbanized (as of 2022), and the large area is covered with forest, indicating a healthy and diverse environment that needs to be conserved and protected.

Using the validation dataset, the performance of the RF-based LULC classification was assessed. Tables 3, 4, 5, and 6 show the result of the accuracy assessment of the LULC maps (Figure 4) that were generated using SR, SR-Ht, SR-LST, and SR-Ht-LST, respectively.

In Table 3, when the SR information was used in LULC classification, the class-based F1-scores ranged from 0.65–0.98, which were observed in agriculture and water, respectively. The other classes including bareland, built-up, forest, and grassland had an F1-score of 0.89, 0.67, 0.90, and 0.77, respectively, resulting in a Macro F1-score of 0.81 with a K of 0.83. When the Ht information was added to SR for LULC classification, the F1-score of bareland, built-up, forest, grassland, agriculture, and water was improved to 0.90, 0.71, 0.92, 0.78, 0.69, and 0.99, respectively, resulting to an improved Macro F1-score of 0.83 and a K of 0.86 (Table 4). The F1-score of the classes was further improved when the LST information was added to the SR and Ht information, as shown in Table 5. The F1-scores of bareland, built-up, forest, grassland, agriculture, and water increased to 0.91, 0.74,
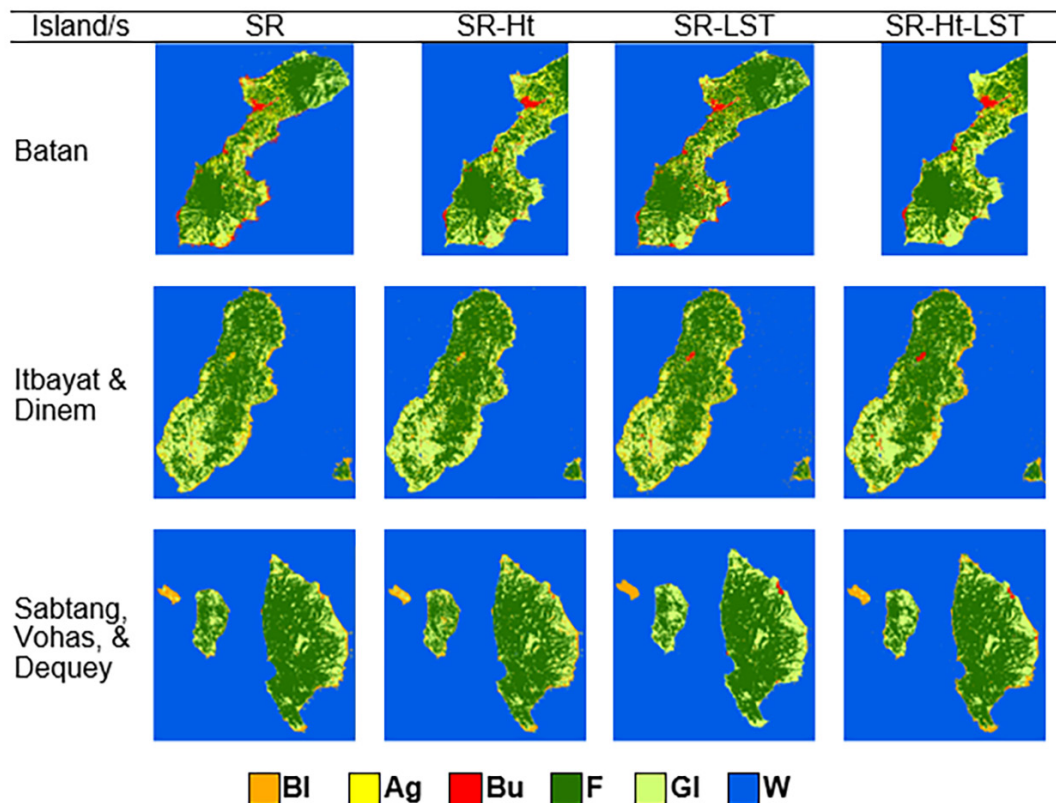


**Figure 4.** RF-based LULC classification using multi-sourced input data.

**Table 3.** Accuracy assessment of the LULC product generated using SR information.

| SR | | Observed classes | | | | | | |
|---|---|---|---|---|---|---|---|---|
| | | Bl | Bu | F | Gl | Ag | W | Total |
| Classified classes | Bl | 1197 | 54 | 24 | 13 | 6 | 8 | 1302 |
| | Bu | 15 | 180 | 27 | 25 | 6 | 6 | 259 |
| | F | 33 | 22 | 1790 | 86 | 71 | 0 | 2002 |
| | Gl | 86 | 9 | 61 | 690 | 59 | 0 | 905 |
| | Ag | 24 | 13 | 93 | 77 | 319 | 2 | 528 |
| | W | 37 | 1 | 0 | 0 | 0 | 1467 | 1505 |
| | Total | 1392 | 279 | 1995 | 891 | 461 | 1483 | 6501 |
| Precision | | 0.92 | 0.69 | 0.89 | 0.76 | 0.60 | 0.97 | |
| Recall | | 0.86 | 0.65 | 0.90 | 0.77 | 0.69 | 0.99 | |
| F1-score | | 0.89 | 0.67 | 0.90 | 0.77 | 0.65 | 0.98 | |

Macro F1-score = 0.81; K = 0.83; overall accuracy = 0.87

**Table 4.** Accuracy assessment of the LULC product generated using SR and Ht information.

| SR-Ht | | Observed classes | | | | | | |
|---|---|---|---|---|---|---|---|---|
| | | Bl | Bu | F | Gl | Ag | W | Total |
| Classified classes | Bl | 1206 | 27 | 5 | 25 | 5 | 7 | 1275 |
| | Bu | 34 | 185 | 0 | 23 | 3 | 0 | 245 |
| | F | 41 | 12 | 1865 | 59 | 61 | 0 | 2038 |
| | Gl | 69 | 33 | 47 | 710 | 54 | 7 | 920 |
| | Ag | 15 | 22 | 78 | 72 | 338 | 0 | 525 |
| | W | 27 | 0 | 0 | 2 | 0 | 1469 | 1498 |
| | Total | 1392 | 279 | 1995 | 891 | 461 | 1483 | 6501 |
| Precision | | 0.95 | 0.76 | 0.92 | 0.77 | 0.64 | 0.98 | |
| Recall | | 0.87 | 0.66 | 0.93 | 0.80 | 0.73 | 0.99 | |
| F1-score | | 0.90 | 0.71 | 0.92 | 0.78 | 0.69 | 0.99 | |

Macro F1-score = 0.83; K = 0.86; overall accuracy = 0.89

**Table 5.** Accuracy assessment of the LULC product generated using SR and LST information.

| SR- LST | | Observed classes | | | | | | |
|---|---|---|---|---|---|---|---|---|
| | | Bl | Bu | F | Gl | Ag | W | Total |
| Classified classes | Bl | 1213 | 17 | 8 | 20 | 7 | 0 | 1265 |
| | Bu | 41 | 200 | 0 | 4 | 14 | 6 | 265 |
| | F | 17 | 15 | 1920 | 38 | 11 | 0 | 2001 |
| | Gl | 55 | 23 | 38 | 758 | 69 | 0 | 943 |
| | Ag | 39 | 13 | 29 | 71 | 360 | 0 | 512 |
| | W | 27 | 11 | 0 | 0 | 0 | 1477 | 1515 |
| | Total | 1392 | 279 | 1995 | 891 | 461 | 1483 | 6501 |
| Precision | | 0.96 | 0.75 | 0.96 | 0.80 | 0.70 | 0.97 | |
| Recall | | 0.87 | 0.72 | 0.96 | 0.85 | 0.78 | 1.00 | |
| F1-score | | 0.91 | 0.74 | 0.96 | 0.83 | 0.74 | 0.99 | |

Macro F1-score = 0.86; K =0.89; overall accuracy = 0.91

**Table 6.** Accuracy assessment of the LULC product generated using SR, Ht, and LST information.

| SR- Ht-LST | | Observed classes | | | | | | |
|---|---|---|---|---|---|---|---|---|
| | | Bl | Bu | F | Gl | Ag | W | Total |
| Classified classes | Bl | 1329 | 2 | 0 | 6 | 10 | 0 | 1347 |
| | Bu | 8 | 241 | 0 | 5 | 1 | 0 | 255 |
| | F | 5 | 12 | 1910 | 23 | 22 | 0 | 1972 |
| | Gl | 37 | 19 | 36 | 821 | 32 | 0 | 945 |
| | Ag | 13 | 5 | 49 | 36 | 396 | 0 | 499 |
| | W | 0 | 0 | 0 | 0 | 0 | 1483 | 1483 |
| | Total | 1392 | 279 | 1995 | 891 | 461 | 1483 | 6501 |
| Precision | | 0.99 | 0.95 | 0.97 | 0.87 | 0.79 | 1.00 | |
| Recall | | 0.95 | 0.86 | 0.96 | 0.92 | 0.86 | 1.00 | |
| F1-score | | 0.97 | 0.90 | 0.96 | 0.89 | 0.83 | 1.00 | |
| Macro F1-score = 0.93; K = 0.94; overall accuracy = 0.95 | | | | | | | | |

0.96, 0.83, 0.74, and 0.99, respectively. The Macro F1-score increased to 0.86 and K increased to 0.89. When the Ht and LST information were both added to SR for LULC classification, the highest F1-score of each class was observed (Table 6). The F1-score of bareland, built-up, forest, grassland, agriculture, and water increased to 0.97, 0.90, 0.96, 0.89, 0.83, and 1.0, respectively, and the Macro F1-score increased to 0.93 and K increased to 0.94.

The F1-score of the classes had an average increase of 0.04 when the Ht information was added to SR for LULC classification and an average of 0.08 when LST was added to SR. An average increase of 0.12 was observed when both the Ht and LST information were added. This indicates that LST has a higher impact than the Ht information on LULC classification. Nevertheless, the highest effect was observed when both the Ht and LST information were simultaneously added to the SR information. The Macro F1-score and K were increased by as much as 2 and 3% when the Ht information was added to SR, as much as 5 and 6% when the LST was added to SR, and as much as 12 and 11% when both the Ht and LST information was included with SR in the LULC classification.

Further, based on Tables 3–6, a varying magnitude of accuracy improvement was observed in each class. When the Ht information was added to SR information, the highest individual increase was observed in both agriculture and built-up with a value of 0.04, followed by forest with a value of 0.02, and then bareland, grassland, and water with an increase of 0.01. As to the effect of the LST, the highest increase was observed in agriculture with a value of 0.09, followed by built-up with a value of 0.07, then both forest and grassland with a value of 0.06, bareland with an increase of 0.02, and lastly, the

water with an increase of 0.01. When both the Ht and LST information was added, the highest increase was observed in built-up with a value of 0.23, agriculture with a value of 0.18, then grassland with 0.12, bareland with 0.08, forest with 0.06, and lastly, water with 0.02. The analysis indicates that the accuracy of water was the most stable among the other classes, whereas the built-up and agriculture suffered the most misclassification when only the SR information is used in LULC classification.

## DISCUSSION

**Comparison of the LULC Products in This Study with the Global-scale LULC Products**
Figures 5 and 6 display the LULC maps of the study sites, which were derived from existing global-scale LULC products such as GLAD and ESRI, respectively. It was previously reported that the global accuracy of GLAD and ESRI LULC products stood at 78.35 and 86%, respectively. However, upon using locally collected ground truth data as the validation dataset, the overall accuracy of the GLAD and ESRI products decreased to 77 and 73%, respectively. This represented a decrease in accuracy of 1.35% for the GLAD product and 13% for the ESRI product. Comparing the Macro F1-score and K, it was found that the accuracy of the GLAD and ESRI LULC products in this study was lower by as much as 20 and 23%, as well as 34 and 30%, respectively, compared to the SR-Ht-LST products.

According to the variation in area coverage for each class depicted in Table 7, it can be observed that both the GLAD and ESRI products underestimated the extent of
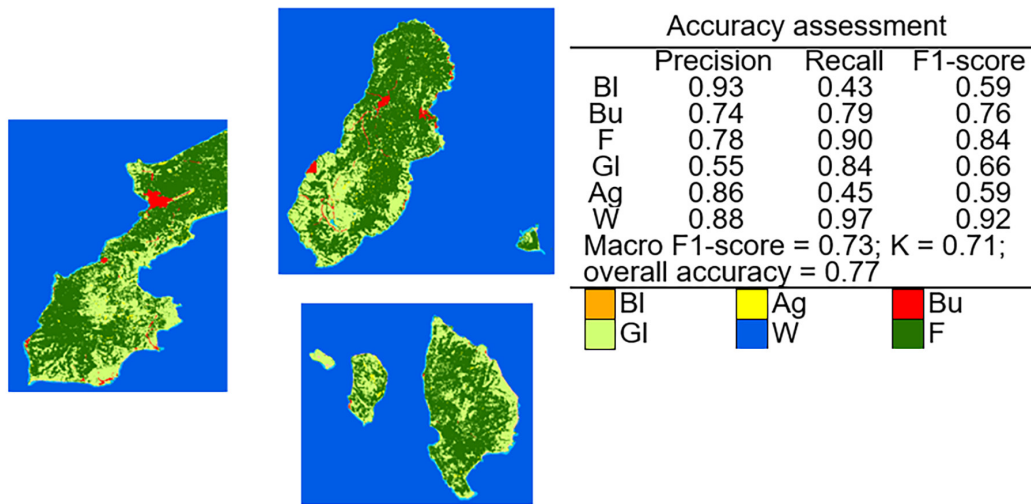
**Figure 5.** LULC map of the study sites based on the GLAD LULC product.
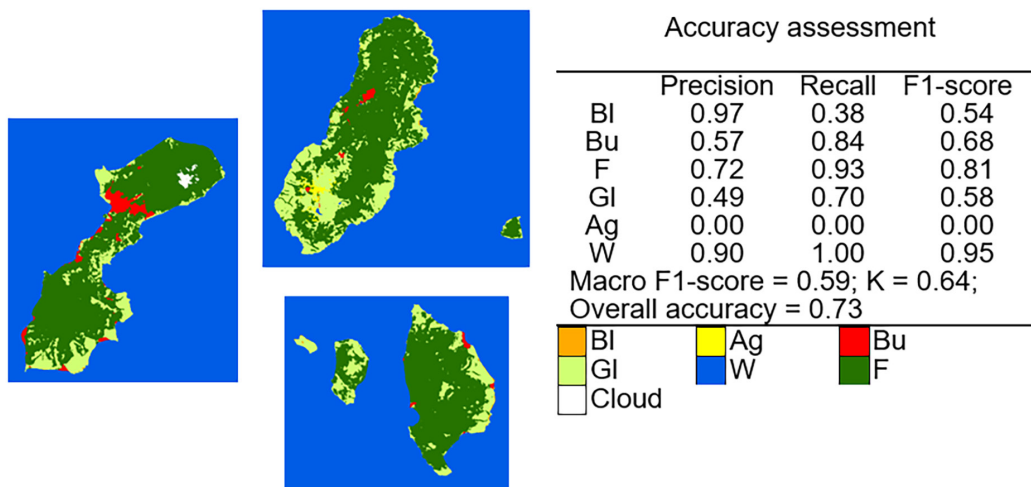


**Figure 6.** LULC map of the study sites based on the ESRI LULC product.

**Table 7.** Comparison of the area percentage distribution of the LULC product in this study (SR-LST-Ht) with the global-scale LULC products (based on the boundary of GLAD LULC product).

| LULC class | Area (%) | | |
|---|---|---|---|
| | This study | Global-scale LULC product | |
| | SR-LST-Ht | GLAD | ESRI |
| Bl | 2.20 | 0.17 | 0.10 |
| Bu | 0.53 | 0.66 | 0.89 |
| F | 20.33 | 21.40 | 23.26 |
| Gl | 8.64 | 10.95 | 8.55 |
| Ag | 1.73 | 0.33 | 0.23 |
| W | 66.58 | 66.50 | 66.96 |
| Cloud cover | | | 0.003 |
| Total | | 100% | |

agriculture and bareland while overestimating the areas of built-up, forest, and water. Specifically, the GLAD product overestimated the area of grassland, whereas the ESRI LULC product underestimated it. In this study, no cloud cover was classified, as it was masked out, and the GLAD product also did not include cloud cover. However, the ESRI product accounted for cloud cover, which occupied an area equivalent to 0.003% of the entire study site.

Accurate information is crucial during LULC planning and the formulation of policies for restoration and protection. While global-scale LULC maps are essential for monitoring land and water resources, there is a trade-off in terms of accuracy. LULC maps generated with broader coverage often exhibit decreased accuracy due to various factors. The generation of LULC maps covering large areas typically involves using satellite

images and reference data acquired at different times, leading to reduced accuracy of the final LULC product (Herold *et al*. 2008; Gong *et al*. 2013). Other contributing factors include atmospheric noise in satellite data images, low spatial resolution of open-sourced data, lack of easily interpretable and automated classifiers, and non-uniformity in classification systems and techniques. Consequently, the accuracy of LULC maps, including global-scale maps, is generally lower, ranging from 67–81% (DeFries *et al.* 1998; Hansen *et al.* 2000; Friedl *et al.* 2010; Gong *et al.* 2013; Chen *et al.* 2015; Buchhorn *et al.* 2019; Sulla-Menashe *et al.* 2019). This lower accuracy results in inconsistent and inaccurate classification when applied to localized contexts (Herold *et al.* 2008; Gong *et al.* 2013), leading to unrealistic and problematic outcomes (Congalton *et al.* 2014; Tsendbazar *et al.* 2015).

In contrast, locally produced LULC maps – despite their limitations in terms of area coverage – often exhibit higher accuracy. Consequently, when accuracy is a critical consideration and the focus is on smaller coverage areas, locally generated LULC maps prove to be more reliable.

**Comparison of the LULC Mapping in This Study with the Other Studies Conducted within the Philippines**

As recalled from the results, the integration of LST and Ht information with the SR of Landsat data improved the overall accuracy of the LULC classification from 89 to 95%. Several LULC monitoring had already been conducted in the Philippines, and the reported overall accuracy ranged from 82.97–90.58%. For instance, Merida and Perez (2017) conducted LULC changes in the three main islands of Batanes – namely, Batan, Itbayat, and Sabtang – from 1989, 1997, 2000, 2007, 2010, and 2016 using the SR of Landsat images and SVM as a classifier. From their analysis, they reported overall accuracies of 87.63, 87.98, 82.97, 84.47, 88.07, and 86.97% for 1989, 1993, 2000, 2007, 2010, and 2016, respectively. Further, they reported an upward trend of forest cover on the island of Batan, whereas a relatively stable forest cover for Sabtang and Itbayat. In Mt. Pulag National Park, Doyog *et al.* (2021) monitored the LULC changes on a 10-year basis from 1990–2020 using the SR of Landsat and Sentinel images and MLC. From their analysis, they have reported overall accuracy of 86.91, 87.43, 89.01, and 90.58% for 1990, 2000, 2010, and 2020, respectively. On the other hand, Clarin *et al.* (2021) used the SR of Landsat images and MLC to perform LULC monitoring in Mactan Island, Cebu and reported overall accuracy of 86.2% for the year 2000 and 86.4% for 2018, whereas Estoque and Murayama (2011) reported overall accuracy of 86.86% (1988), 87.18% (1998), and 89.10% (2009) of the land use and cover of Baguio City produced using remote sensing images and MLC.

To summarize, the SR of Landsat images was the only feature that was used in the LULC classification of the previous studies. The overall accuracy in this study when using only the SR of Landsat images is comparable with the reported studies. However, the addition of the LST and Ht information made the overall accuracy of the LULC performed in this study superior.

The use of SR features of satellite images can provide reliable LULC classification results. However, issues are still observed in separating LULC classes from each other. For instance, the study by Merida and Perez (2017) showed that built-up was classified as a barren area. In this case, with the addition of Ht information to the SR features, it can be separated since barren areas are likely to have low Ht values, whereas built-up – especially buildings – have Ht values higher than barren areas. Therefore, the addition of other features like Ht and LST is an advantage to achieving higher accuracy and more reliable LULC classification.

As to the observed trends of LULC changes in the Philippines, the decreasing trend is usually observed in natural LULC – especially the forest, grassland, and bareland areas – and an increasing trend in human-intervened LULC like agriculture and built-up areas. It is observed that the decrease in forest cover, grassland, and bareland areas is mainly due to agriculture and built-up expansion. Mitigating actions are, therefore, needed for the protection of the environment while catering to the needs of the present and future populations.

## CONCLUSION

This study demonstrated the utilization of multi-sourced data – including SR, Ht, and LST – in RF-based LULC classification. The integration of Ht and LST information positively influenced the accuracy of the RF classifier when using Landsat imagery for LULC classification. Notably, the addition of Ht and LST information to SR before LULC classification significantly improved the accuracy. By incorporating Ht and LST information into the SR data, the RF-based LULC classification achieved optimal performance, yielding a Macro F1-score of 0.93 and a K value of 0.94. The inclusion of Ht and LST resulted in a 12% increase in Macro F1-score and an 11% increase in K when compared to the classification based solely on SR. These findings highlight that the simultaneous use of SR, Ht, and LST as input data allows the RF-based LULC classification to attain the highest level of accuracy. The outcomes of this study provide a LULC classification protocol that incorporates reliable information for assessing the state of the Earth's natural resources.

## ACKNOWLEDGMENTS

## STATEMENT ON CONFLICT OF INTEREST

The authors declare no conflict of interest.

## REFERENCES

BAIG MF, MUSTAFA MRU, BAIG I, TAKAIJUDIN HB, ZESHAN MT. 2022. Assessment of Land Use Land Cover Changes and Future Predictions Using CA-ANN Simulation for Selangor, Malaysia. Water 14(3): 402. https://doi.org/10.3390/w14030402

BASHEER S, WANG X, FAROOQUE AA, NAWAZ RA, LIU K, ADEKANMBI T, LIU S. 2022. Comparison of Land Use Land Cover Classifiers Using Different Satellite Imagery and Machine Learning Techniques. Remote Sens 14: 4978. https:// doi.org/10.3390/rs14194978

BREIMAN L. 2001. Random Forests. Mach Learn 45: 5–32. http://doi.org/10.1023/A:1010933404324

BUCHHORN M, SMETS B, BERTELS L, LESIV M, TSENDBAZAR NE, HEROLD M, FRITZ S. 2019. Copernicus Global Land Service: Land Cover 100 m: Epoch 2015: Globe; (Version V2.0.2); Zenodo: Geneva, Switzerland.

CHEN J, CHEN J, LIAO A, CAO X, CHEN L, CHEN X, HE C, HAN G, PENG S, LU M. 2015. Global Land Cover Mapping at 30 m Resolution: a POK-based Operational Approach. ISPRS J. Photogram. Remote Sens 103: 7–27.

CLARIN DC, DY DT, DIOLA AG. 2021. Evaluation of Land Use Land Cover Change due to Urbanization in Mactan Island, Cebu, Using Landsat Data. Manila Journal of Science 14: 86–103.

CONGALTON GR, GU J, YADAV K, THENKABAIL P, OZDOGAN M. 2014. Global Land Cover Mapping: a Review and Uncertainty Analysis. Remote Sens 6: 12070–12093. https://doi.org/10.3390/rs61212070

DA SILVA VS, SALAMI G, DA SILVA MIO, ARAÚJO SILVA E, MONTEIRO JUNIOR JJ, ALBA E. 2020. Methodological evaluation of vegetation indexes in land use and land cover (LULC) classification. Geol Ecol Landsc 4(2): 159–169. https://doi.org/10.1080/24749508.2019.1608409

DEFRIES RS, HANSEN MC, TOWNSHEND JRG, SOHLBERG RS. 1998. Global land cover classifications at 8 km spatial resolution: the use of training data derived from Landsat imagery in decision tree classifiers. Int J Remote Sens 19: 3141–3168.

DISPERATI L, VIRDIS SG. 2015. Assessment of land-use and land-cover changes from 1965 to 2014 in Tam Giang-Cau Hai Lagoon, central Vietnam. Appl Geogr 58: 48–64.

DOYOG ND, LUMBRES RIC, BAOANAN ZG. 2021. Monitoring of Land Use and Land Cover Changes in Mt. Pulag National Park Using Landsat and Sentinel Imageries. Philipp J Sci 150(4): 723–734.

ESTOQUE RC, MURAYAMA Y. 2011. Spatio-temporal Urban Land Use/Cover Change Analysis in a Hill Station: The Case of Baguio City, Philippines. Procedia Soc Behav Sci 21: 326–335. https://doi.org/10.1016/j.sbspro.2011.07.016

[FAO] Food and Agriculture Organization. 2016. Land cover classification system. Rome, Italy.

FRIEDL MA, SULLA-MENASHE D, TAN B, SCHNEIDER A, RAMANKUTTY N, SIBLEY A, HUANG XM. 2010. MODIS Collection 5 Global Land Cover: Algorithm Refinements and Characterization of New Datasets. Remote Sens Environ 114(1): 168–182. http://dx.doi.org/10.1016/j.rse.2009.08.016

GEBREJEWERGS A, ATINKUT M, ATKILT G. 2018. Land-use land-cover classification analysis of Giba catchment using hyper temporal MODIS NDVI satellite images. Int J Remote Sens 39(3): 810–821, https://doi.org/10.1080/01431161.2017.1392639

GISLASON PO, BENEDIKTSSON JA, SVEINSSON JR. 2006. Random forests for land cover classification. Pattern Recognit Lett 27(4): 294–300. https://doi.org/10.1016/j.patrec.2005.08.011

GHIMIRE B, ROGAN J, MILLER J. 2010. Contextual land-cover classification: incorporating spatial dependence in land-cover classification models using random forests and the Getis statistic. Remote Sens Lett 1(1): 45–54. https://doi.org/10.1080/01431160903252327

GONG P, WANG J, YU L, ZHAO Y, ZHAO Y, LIANG L, NIU Z *et al.* 2013. Finer Resolution Observation and Monitoring of Global Land Cover: First Mapping Results with Landsat TM and ETM+ Data. Int J Remote

Sens 34(7): 2607–2654. https://doi.org/10.1080/0143 1161.2012.748992

GUO L, CHEHATA N, MALLET C, BOUKIR S. 2011. Relevance of airborne lidar and multispectral image data for urban scene classification using Random Forests. ISPRS J Photogram Remote Sens 66(1): 56–66. https://doi.org/10.1016/j.isprsjprs.2010.08.007

GXUMISA A, BREYTENBACH A. 2017. Evaluating Pixel *vs.* Segmentation based Classifiers with Height Differentiation on SPOT 6 Imagery for Urban Land Cover Mapping. S Afr J Geomat 6(3): 436–448. http://dx.doi.org/10.4314/sajg.v6i3.12

HANSEN MC, DEFRIES RS, TOWNSHEND JRG, SOHLBERG R. 2000. GLC classification at 1km spatial resolution using a classification tree approach. Int J Remote Sens 21(6–7): 1331–1364

HANSEN MC, POTAPOV PV, PICKENS A, TYU-KAVINA A, HERNANDEZ SERNA A, ZALLES V, TURUBANOVA S, KOMMAREDDY I, STEHMAN SV, SONG X, KOMMAREDDY A. 2022. Global land use extent and dispersion within natural land cover using Landsat data. Environ Res Lett 17: 034050. https://doi.org/10.1088/1748-9326/ac46ec

HAVENS S, MARSHALL H, PIELMEIER C, ELDER K. 2013. Automatic grain type classification of snow micro penetrometer signals with random forests. IEEE Trans Geosci Remote Sens 51(6): 3328–3335. https://doi.org/10.1109/TGRS.2012.2220549

HEROLD M, MAYAUX P, WOODCOCK C, BACCINI A, SCHMULLIUS C. 2008. Some Challenges in Global Land Cover Mapping: an Assessment of Agreement and Accuracy in Existing 1 km Datasets. Remote Sens Environ 112: 2538–2556. https://doi.org/10.1016/j.rse.2007.11.013

KARRA K, KONTGIS C, STATMAN-WEIL Z, MAZZARIELLO JC, MATHIS, M, BRUMBY SP. 2021. Global Land Use/Land Cover with Sentinel 2 and Deep Learning. IEEE: Manhattan, NY, USA. p. 4704–4707.

LI G, LU D, MORAN E, SANT'ANNA SJS. 2012. Comparative analysis of classification algorithms and multiple sensor data for land use/land cover classification in the Brazilian Amazon. J Appl Rem Sens 6(1): 061706. https://doi.org/10.1117/1.JRS.6.061706

MERIDA HCE, PEREZ GJP. 2017. Assessing Land Cover/Land Use Change In A Small Island Protected Area through Google Earth Engine: the Case of Batanes. 38th Asian Conference on Remote Sensing (ACRS 2017) – Space Applications: Touching Human Lives; 23–27 Oct 2017; New Delhi, India.

MI J, YANG Y, ZHANG S, AN S, HUO H, HUA Y, CHEN F. 2019. Tracking the Land Use/Land Cover Change in an Area with Underground Mining and reforestation *via* Continuous Landsat Classification. Remote Sens 11: 1719. https://doi.org/10.3390/rs11141719

NITZE I, BARRETT B, CAWKWELL F. 2015. Temporal optimisation of image acquisition for land cover classification with Random Forest and MODIS time-series. Int J Appl Earth Obs Geoinf 34: 136–146. https://doi.org/10.1016/j.jag.2014.08.001

POTAPOV P, LI X, HERNANDEZ-SERNA A, TYU-KAVINA A, HANSEN MC, KOMMAREDDY A, PICKENS A, TURUBANOVA S, TANG H, SILVA CE, ARMSTON J, DUBAYAH R, BLAIR JB, HOFTON M. 2021. Mapping global forest canopy height through integration of GEDI and Landsat data. Remote Sens Environ 112165. https://doi.org/10.1016/j.rse.2020.112165

PUISSANT A, ROUGIER S, STUMPF A. 2014. Object-oriented mapping of urban trees using Random Forest classifiers. Int J Appl Earth Obs Geoinf 26(1): 235–245. https://doi.org/10.1016/j.jag.2013.07.002

[PSA] Philippine Statistics Authority. 2020. Census of Population. 2020. "Region II (Cagayan Valley)". Total population by Province, City, Municipality, and *Barangay*. Quezon City, Philippines.

SERTEL E, EKIM B, ETTEHADI OSGOUEI P, KABADAYI ME. 2022. Land Use and Land Cover Mapping Using Deep Learning Based Segmentation Approaches and VHR Worldview-3 Images. *Remote Sens* 14(18): 4558. https://doi.org/10.3390/rs14184558

SINHA S, KANT SHARMA L, SINGH NATHAWAT M. 2015. Improved Land-use/Land-cover classification of semi-arid deciduous forest landscape using thermal remote sensing. Egypt. J Remote Sens Space Sci 18(2): 217–233. https://doi.org/10.1016/j.ejrs.2015.09.005

SONG K, WANG Z, LIU Q, LIU D, ERMOSHIN VV, GANZEI SS, ZHANG B, REN C, DU J. 2011. Land use/land cover (LULC) classification with MODIS time series data and validation in the Amur River Basin. Geogr Nat Resour 32: 9–15. https://doi.org/10.1134/S1875372811010021

SULLA-MENASHE D, GRAY JM, ABERCROMBIE SP, FRIEDL MA. 2019. Hierarchical mapping of annual global land cover 2001 to present: The MODIS Collection 6 Land Cover product. Remote Sens Environ 222: 183–194.

TARAZONA Y, MIYASIRO-LÓPEZ M. 2020. Monitoring tropical forest degradation using remote sensing: challenges and opportunities in the Madre de Dios region,

Peru. Remote Sens Appl: Soc Environ 19: 100337.

TSENDBAZAR N, BRUIN S, HEROLD M. 2015. Assessing Global Land Cover Reference Datasets for Different User Communities. ISPRS J Photogram Remote Sens 103: 93–114. https://doi.org/10.1016/j.isprsjprs.2014.02.008

VILAR L, HERRERA S, TAFUR-GARCÍA E, YEBRA M, MARTÍNEZ-VEGA J, ECHAVARRÍA P, MARTÍN MP. 2021. Modelling wildfire occurrence at regional scale from land use/cover and climate change scenarios. Environ Model Softw 145: 105200. https://doi.org/10.1016/j.envsoft.2021.105200

WIEDERKEHR NC, GAMA FF, NEVES E CASTRO PB, BISPO PC, BALZTER H, SANO E, LIESENBERG V, SANTOS J, MURA J. 2020. Discriminating Forest Successional Stages, Forest Degradation, and Land Use in Central Amazon Using ALOS/PALSAR-2 Full-Polarimetric Data. Remote Sens 12: 3512. https://doi.org/10.3390/rs12213512

XIA J, CHANUSSOT J, DU P, HE X. 2015. Spectral-spatial classification for hyperspectral data using rotation forests with local feature extraction and Markov random fields. IEEE Trans Geosci Remote Sens 53(5): 2532–2546. https://doi.org/ 10.1109/TGRS.2014.2361618

XIE Z, CHEN Y, LU D, LI G, CHEN E. 2019. Classification of Land Cover, Forest, and Tree Species Classes with ZiYuan-3 Multispectral and Stereo Data. Remote Sens 11: 164.

YUMUL G, CRUZ N, SERVANDO N, DIMALANTA C. 2011. Extreme Weather Events and Related Disasters in the Philippines 2004–08: a Sign of What Climate Change Will Mean? Disasters 35(2): 362–382. https://doi.org/10.1111/j.1467-7717.2010.01216.x

ZANTER K. 2019. Landsat 8 (L8) Data Users Handbook. LSDS-1574 Version 5, 1–106.

ZHANG J, KEREKES J. 2011. Unsupervised urban land-cover classification using WorldView-2 data and self-organizing maps. IEEE International Geoscience and Remote Sensing Symposium, Vancouver, BC, Canada. p. 150–153. https://doi.org/10.1109/IGARSS.2011.6048920